



On the transformation mechanism of polyethylene glycol- and citrate-coated silver nanocolloids under sunlight exposure

Sylvie Motellier  · Isabella Römer ·
Nathalie Pélissier · Eugenia Valsami-Jones

Received: 19 March 2019 / Accepted: 13 June 2019 / Published online: 22 July 2019
© Springer Nature B.V. 2019

Abstract As the use of nanomaterials continues to increase, their release into the environment is also expected to increase. During the use phase of nano-enhanced products containing silver nanoparticles (Ag NPs) or after the release of Ag NPs in the environment, the latter are likely to be altered by the conditions they will encounter, such as sunlight irradiation. In this work, suspensions of citrate-stabilized and PEG-stabilized Ag NPs of around 20 nm in diameter were synthesized and aged for a week in a climatic chamber under controlled temperature (40 °C) and sunlight irradiation. The suspensions were analyzed by UV/visible spectroscopy, asymmetric flow field flow fractionation—inductively coupled plasma mass spectrometry (AF4-ICP-MS), dynamic light scattering (DLS), and transmission electron microscopy (TEM). We found that the electrostatic-stabilizing citrate promoted particle morphology changes with the emergence of a transient and minor secondary population of truncated 2D prisms (110–120 nm in size) but postponed the final

sedimentation step. Conversely, the initial protecting role of the steric-stabilizing PEG was reduced by the photodegradation of the polymer chains and eventually favored inter-particle bridging resulting in aggregation and sedimentation. It is hypothesized that the bridging process proceeds via PEG chain interpenetration between two adjacent particles and reduction by the polymer photodegradation products of the Ag⁺ ions generated by oxidative dissolution.

Keywords Silver nanoparticles · Coating · Aging · Environmental fate · Ecotoxicity

Introduction

Silver nanoparticles (Ag NPs) are now incorporated in many consumer products such as printed electronics with functional inks or fabrics with antibacterial properties (Mitrano et al. 2015; Rajan et al. 2016; Reidy et al. 2013). In 2015, more than 400 products containing Ag NPs were listed in the Nanotechnology Consumer Products Inventory, with an overall marked enhancement in applications (Vance et al. 2015). This large amount of uses for Ag NPs increases the potential risk of discharge to the environment, which is a real concern given the undisputed biological adverse effects related to Ag NP solubility.

Contamination processes of the environment may occur throughout the life cycle of Ag NPs, from their synthesis to their incorporation into products, use phase, recycling, and disposal. Direct release (from paints applied on outdoor facades for instance (Kaegi et al. 2010)) or release through waste streams (e.g., after

Electronic supplementary material The online version of this article (<https://doi.org/10.1007/s11051-019-4584-4>) contains supplementary material, which is available to authorized users.

S. Motellier (✉) · N. Pélissier
Commissariat à l’Energie Atomique et aux Energies Alternatives,
DRT/LITEN/DTNM/S2CE/L2N, Laboratory of
Nano-characterization and Nano-safety, University Grenoble
Alpes, 17 Avenue des Martyrs, 38054 Grenoble, France
e-mail: Sylvie.motellier@cea.fr

I. Römer · E. Valsami-Jones
School of Geography, Earth and Environmental Sciences,
University of Birmingham, Edgbaston, Birmingham B15 2TT,
UK

household laundering of textiles (Mitrano et al. 2014)) yields predicted concentrations of Ag NPs in the ng L^{-1} range for surface waters (Fabrega et al. 2011).

Once in the environment, Ag NPs will experience concurrent transformations based on the physico-chemical conditions of the medium (pH, aerobic/anaerobic, nature and concentration of salts and interfering organic reagents, light/darkness, etc.) and on the particles themselves (coating, size and shape, crystallinity, etc.): redox processes, dissolution, aggregation/precipitation, photodegradation. As an example, a significant amount of Ag released from wastewater treatment plants was found to have transformed into sulfidized nanoAg species (Azodi et al. 2016). Among the numerous parameters that strongly affect the stability of Ag NPs and, consequently, their (eco)toxicological impact (Misra et al. 2012), the capping agent aiming at controlling the synthesis of the particles and protecting them from dissolution and agglomeration was found to be an important factor (Tejamaya et al. 2012). Citrate is commonly used as a charge repulsion stabilizer (Römer et al. 2011), which is weakly bound to the core, while polymers are chosen to stabilize the NPs sterically. In this instance, polyethylene glycol (PEG) is an interesting candidate because it is water-soluble, which is an essential property for efficient stabilization in aqueous medium. It also preserves the biological activity of the material and reduces toxicity due to the fact that it is known to be well tolerated by the human body (Pinzaru et al. 2018).

During the use phase of the nano-enhanced products, Ag NPs are likely to be altered by the conditions they will encounter, such as sunlight irradiation for textiles which are regularly worn outdoor. Light-induced growth/transformation of Ag NPs is a well-known phenomenon that has been used for Ag NP synthesis (Jin et al. 2003; Krajczewski et al. 2015; Tang et al. 2015), including directly in polymeric matrices (Chiolerio and Sangermano 2012). Recent studies have indicated that Ag nano-enhanced textiles which first underwent a UV exposure had fewer subsequent speciation changes upon laundering the fabric (Mitrano et al. 2016). In a previous work, citrate-stabilized Ag NPs of different sizes were found to behave differently when aged for a week in a climatic chamber under artificial sunlight (Motellier et al. 2018). Beside the role of the particle size, the influence of the coating on the fate of Ag NPs exposed to light is controversial: while Li and Lenhart found that Tween 80 (sterically)-stabilized Ag NPs dissolved more rapidly under artificial sunlight exposure than did bare or

citrate-coated NPs (Li and Lenhart 2012), Li et al. found that the concentration of Ag^+ ion was more important for bare NPs followed by PVP-coated and citrate-coated Ag NPs after 5 h of irradiation (Li et al. 2013).

In order to address this last point and try to clarify the role of the particle coating on the fate of suspensions of silver nanoparticles when they are exposed to sunlight irradiation, citrate- and PEG-coated Ag NPs of 20 nm in size were irradiated in a climatic chamber and the kinetics of the particle degradation was followed by various techniques. Transmission electron microscopy (TEM) and dynamic light scattering (DLS) were proposed as reference techniques for the characterization of particle morphology and population size distribution, respectively. Because of the characteristic absorbance spectra of colored Ag NPs due to their surface plasmon resonance, UV/visible spectroscopy has been extensively used for the monitoring of Ag NP synthesis and morphology evolution under various solicitations (Callegari et al. 2003; Jiang et al. 2010; Jin et al. 2001; Maillard et al. 2003) and was evaluated in the present study. Asymmetric flow field flow fractionation (AF4) allows the fractionation of colloidal particles according to their size (Baalousha et al. 2011), which is a valuable tool when dealing with complex colloidal populations. It has been successfully coupled to UV/visible detection for the characterization of the stability of Ag NPs in several media (Cumberland and Lead 2009; Römer et al. 2011). However, on-line UV/visible detection is not specific and suffers from numerous interferences, particularly for polymer-capped Ag NPs where the polymer may potentially change its color (from transparent to yellow) upon degradation (Yu et al. 2014). The use of an on-line elemental technique like inductively coupled plasma mass spectrometry (ICP-MS) is an interesting alternative that provides specific quantitative detection of metal-based nanoparticles (Dubascoux et al. 2010; Hagendorfer et al. 2012). AF4-ICP-MS has been used to characterize the stages of suspension evolution under irradiation with the aim to evaluate its interest compared to the more conventional techniques cited above.

Experimental

Chemicals

Ultrapure (UP) water (Milli-Q, Millipore, Billerica, USA) was used throughout the experimental work.

Nitric acid (HNO₃ Suprapur quality, 65 wt%) and sodium hydroxide (NaOH Suprapur quality, monohydrate) were from Merck (Darmstadt, Germany). Sodium nitrate, sodium citrate, silver nitrate, sodium borohydride, and thiolated PEG (PEG-SH, MW5000) were from Aldrich (St Louis, USA). The ionic Ag standard for ICP (1000 mg L⁻¹ in 2% HNO₃ Tracecert grade) was from Fluka (Sigma-Aldrich, St Louis, USA). Suspensions of citrate-stabilized Ag NPs (20, 30, 40, 50, 60, 70, 80, and 90 nm) used for the calibration of the AF4 were provided by the Joint Research Center (JRC, Ispra, Italy).

Synthesis of Ag NPs

Two aqueous dispersions of silver nanoparticles (electrostatically stabilized citrate- or sterically stabilized polyethylene glycol (PEG)-coated) of ca. 20 nm in size and ~40 mg L⁻¹ in concentration were synthesized according to the protocol described in detail in the supporting information (SI). They will be referred to as Ag Cit and Ag PEG. Basically, Ag Cit particles were prepared from a standard reduction of a silver salt in sodium citrate (Römer et al. 2011), cleaned by ultrafiltration, re-dispersed in citrate solution to avoid further growth, and concentrated by ultrafiltration to 44 mg L⁻¹. Once the citrate-capped Ag NPs were produced and washed, an aliquot of citrate-stabilized Ag NPs was converted to PEG-coated NPs by addition of thiolated PEG-SH to coat the particles with 4 molecules of PEG-SH per nm² (Fernández-López et al. 2009; Tejamaya et al. 2012). DLS and UV/visible were used to confirm that the citrate-coated Ag NPs had been converted into PEGylated Ag NPs with no further changes. Ag PEG particles were then purified, re-dispersed in PEG-SH solution, and concentrated to a final concentration of 38 mg L⁻¹. The particles were characterized by TEM to measure their core size. The Ag Cit mean diameter was estimated to be $D_{\text{Ag Cit, TEM}} = 21.2 \pm 7.0$ ($n = 100$) and that of Ag PEG was $D_{\text{Ag PEG, TEM}} = 21.3 \pm 5.7$ ($n = 124$).

All suspensions (stock and aliquots from time points of aging) were homogenized 5 to 10 s with a vortex mixer before dilution to the target concentrations, depending on the analytical method to be used. Sonication was avoided as it was found to promote agglomeration of the particles, particularly for the smallest ones, and damage PEG chains (Murali et al. 2015).

Accelerated weathering testers

The aging experiments were performed in a climatic test chamber (QSUN model Xe-3, QLab) equipped with xenon arc lamps and a Daylight-Q filter that reproduce the full solar spectrum. The temperature was controlled via a black panel sensor to provide an estimate of the maximum temperature that the suspension samples may reach. The chamber air temperature was controlled simultaneously using a simple thermometer. Humidity was monitored during the whole experiment (50%), although it was not relevant in this experiment. The weathering conditions used for the aging experiments were adapted from the guidelines of ISO standards 16474-1:2013 and 16474-2:2013. The irradiance selected value of 1.44 W/m² (at 420 nm) simulated direct sunlight at noon in the summer. It was applied in a continuous manner to increase the rate of aging of the Ag nano-suspensions. This rate is highly material-dependent and no single acceleration factor can be applied. The chamber air temperature was set to a value of 40 °C (70 °C black panel).

All suspensions were aged without dilution. Thirty milliliters of each suspension were placed in glass vials sealed with PTFE liner-screw caps and aged in the test chamber. At selected times, 3-mL aliquots were withdrawn from the vials, deposited in smaller glass vials, and stored at 4 °C until further characterization. A dark control at 40 °C but without irradiance revealed no changes in the samples, which remained identical to the pristine suspensions.

It should be noted that the transmittance cut-off of borosilicate glass is around 300 nm, so that the use of glass vials decreases sample exposure to the UV part of the solar spectrum which, in turn, is supposed to decrease the rate of particle transformation compared with direct exposure to the lamps.

Characterization methods

UV/visible spectroscopy Spectra were acquired with a double beam UV/visible/NIR spectrophotometer (UV 3100, Shimadzu Corporation) equipped with a deuterium lamp and a tungsten lamp. The slit was set to 2 nm. The suspensions were diluted in UP water by a factor of 6 (Ag Cit) or 10 (Ag PEG) to ensure that the maximum absorbance is below 1 A.U.

Size and zeta potential Hydrodynamic diameters (D_h) and zeta potentials (ZP) were acquired using a Zetasizer NanoZSP (Malvern Instruments Ltd., Worcs, UK). Size measurements, expressed as the intensity weighted z-average hydrodynamic diameters determined by the cumulant method, were done at an angle of 173° (backscatter) while ZP measurements were done at 13° with reference to the 633-nm laser beam. The temperature was set at 25°C . Standard 60-nm polystyrene latex beads (Magsphere) and a ZP transfer standard of -42 mV (Malvern) were used for instrument calibration. Measurements were performed at each time point after dilution by a factor of 10 (Ag NP final concentration of $\sim 4\text{ mg L}^{-1}$) in 1 mM NaNO_3 . The sample pH was adjusted to 6.5 ± 0.5 by addition of HNO_3 or N_2 -degassed NaOH.

AF4-ICP-MS Asymmetric flow field-flow fractionation was performed using a device composed of a metal-free HPLC system (1260 Infinity, Agilent Technologies, Santa Clara, USA), a flow controller (Eclipse AF4), and a separation channel (275 mm long, 50 mm wide, and height defined by a 350- μm thick spacer), both from Wyatt Technology (Dernbach, Germany). The semi-permeable membrane was made of regenerated cellulose (RC) with a porosity of 10 kDa (Superon, Dernbach, Germany). The injection volume was $50\text{ }\mu\text{L}$. The separation method (see SI, Table SI-1) was optimized in the course of a previous study (not reported here). The AF4 system was coupled with two on-line detectors: a multi-angle laser light scattering (MALLS) detector (Dawn Heleos II, Wyatt Technology) and an inductively coupled plasma-mass spectrometer (7700 x ICP-MS, Agilent Technologies, Santa Clara, USA). The scattered light signal was recorded at an angle of 90° on the MALLS detector. The ICP-MS was equipped with a sample introduction inert sapphire kit (micromist PFA nebulizer, low-condensation PFA spray chamber, and sapphire injector), an o-ring-free quartz torch, and Pt-sampler and skimmer cones. Operating conditions are listed in Table SI-2 of the supplementary information (SI). Data acquisition was done in TRA mode with a dwell time of 1 s for ^{107}Ag . The effluent from the channel was injected into the ICP-MS by pumping it through a capillary tubing with the help of the built-in peristaltic pump at a flow rate of 0.37 mL min^{-1} ; the complementary flow was eluted to waste via a T connector. A very complete description of the technique can be found in (Giddings 1993). The AF4 eluent was

composed of sodium hydroxide at a pH adjusted to 10 and filtered at $0.1\text{ }\mu\text{m}$. Calibration (size versus elution time) was performed by injecting suspensions of mono-disperse 20 to 90 nm Ag NPs in the same experimental conditions so that the diameter from the AF4 fractograms (D_f) directly refers to the geometric diameter here based on TEM estimates provided by the supplier of the Ag NPs used for calibration. The samples were diluted by a factor of 40 in UP water prior to injection to reach an injected Ag NP concentration of $\sim 1\text{ mg L}^{-1}$.

TEM The NPs were observed with a TEM apparatus (Tecnai Osiris, FEI, Hillsboro, USA) equipped with a high-angle annular dark-field (HAADF) detector and an energy dispersive spectroscopy (EDS) microanalysis system (Esprit, Bruker Nano GmbH, Berlin, Germany) connected to four quadrant silicon drift detectors (ChemiStem technology, FEI). The acceleration voltage was 200 kV. Three microliters of samples were deposited on a 400-mesh copper grid covered with a carbon film. The droplets were left for a few minutes for particle settlement, and the liquid was drawn off by using absorbing paper. The grid was then immediately transferred to a vacuum chamber to avoid any subsequent alteration in air until it was analyzed. The average diameter was estimated from the images using ImageJ software freely available at <http://imagej.nih.gov/ij>.

Results and discussion

UV/visible spectroscopy

The most apparent change with exposure time is the color of the suspension, as seen in Fig. 1 (top). Ag Cit evolved to a greenish shade of grey (24–48 h) before sedimentation (220 h), which has been observed before (Römer et al. 2016). The evolution was faster for Ag PEG, with a black precipitate occurring within 2 days and leaving a clear supernatant. These changes were due to particle alteration in size/morphology and aggregation/agglomeration state.

Color changes can be monitored by UV/visible spectrophotometry (Fig. 1 (bottom)). Aging of Ag Cit resulted in a decrease and a broadening in the intensity of the major plasmon resonance band ($\lambda_{\text{max}} = 396\text{ nm}$) concomitantly with a red shift ($\lambda_{\text{max}} = 413\text{ nm}$ after 220 h), as shown in Fig. 2. A second absorption band emerged

between 500 and 800 nm. The red shift of the main absorption band reflects transformations of the particles due to an increase in the primary particle size (Zhang et al. 2013) and/or the formation of aggregates while the secondary band in the red part of the spectrum is significant of the formation of new species of high aspect ratios (Callegari et al. 2003; Jin et al. 2001). In general, the broadening of peaks can be due to a slow sharp transformation or a growth in size distribution, the appearance of a second peak can be due to shape changes and the formation of triangles, absorbance at ~ 688 nm corresponds to the in-plane dipole plasmon resonance modes of silver nanoprisms (Römer et al. 2016; Zou et al. 2015).

Ag PEG behaved quite differently: only an overall decrease in the main band height ($\lambda_{\max} = 397$ nm to 402 nm after 24 h) was observed (no significant shift and no secondary band) with aging time. This type of spectrum profile evolution has been assigned to dissolution (Yu et al. 2014) or to some dimerization/aggregation processes in previous studies (Krajczewski et al. 2014; Römer et al. 2013) leading to a simple decrease in the concentration of the suspended primary particles and finally sedimentation. The global increase of the baseline level of absorbance in the whole visible region, which was observed for all Ag suspensions after 8 h of exposure, confirmed the occurrence of black (probably larger) particles in the suspensions.

Size and zeta potential

The size distributions of the silver suspensions in NaNO_3 1 mM and at near neutral pH are presented in Fig. 3a. Ag Cit was polydisperse (dispersity of 0.45 ± 0.03) and showed an initial z -average hydrodynamic diameter of 38.1 ± 1.5 nm. Little evolution was observed with exposure time. This is consistent with the slight change of color and the small decrease in the plasmon resonance band of the absorbance spectrum. The changes were much more significant in the case of the PEG-coated particles. Starting from the pristine population with a size of $D_h = 67.4 \pm 0.2$ nm and a polydispersity of 0.25 ± 0.01 (less polydisperse than Ag Cit), the hydrodynamic diameter decreased regularly until it reached that of the citrate-stabilized Ag NPs at 8 h of aging. At aging times after 24 h, the D_h increased drastically, reflecting major agglomeration/aggregation processes, in agreement with the UV/visible absorbance

spectra and the sedimentation of a black deposit in the vial.

The hydrodynamic diameters measured were larger than the diameters obtained by TEM, which is in accordance with the electrical double layer thickness characterized by the Debye length ($k^{-1} = 9.5$ nm in 1 mM NaNO_3 electrolyte) for Ag Cit. The larger size shift in the case of Ag PEG was assigned to the layer of polymer chains grafted on the particle surface (Jokerst et al. 2011; Lee et al. 2009; Levin et al. 2006; Marsh et al. 2003); for 5000 MW PEG, the Flory radius is 6.7 nm (Lee et al. 2009; Levin et al. 2006). Since the grafting density (4 molecules of PEG-SH per nm^2) induced a mean distance between the grafting points shorter than the Flory radius, the chain conformation was supposed to be mainly of the “brush” type (Jokerst et al. 2011), with a calculated thickness of the brush of 23.7 nm (Lee et al. 2009).

Concerning ZP measurements (Fig. 3b), no significant differences were observed related to the aging process for the citrate-coated Ag NPs. All values lied between -35 mV and -45 mV at near-neutral pH, independent of the exposure time. PEG-coated Ag NPs displayed a less negative ZP and a clear evolution from -24 mV to -38 mV at 220 h of exposure, close to the ZP values of Ag Cit. From this, we can infer that the surface characteristics of the final “products” obtained were very close to one another, regardless of the stabilizing agent of the original particles. In other words, the PEG coating was most probably seriously damaged or even destroyed during this process.

AF4-ICP-MS

Fractograms of the studied Ag NPs suspensions at different exposure times of the aging kinetics are presented in Fig. 4, showing two on-line detector signals (ICP-MS and MALLS).

Concerning Ag Cit, the peak that corresponded to the main population decreased steadily in size. Simultaneously, the mean diameter (D_h , geometric, based on external elution time calibration) approximately doubled, from 26 nm for the pristine particles to 47 nm at the end of the aging experiment (according to the ICP-MS fractogram profiles). The width of the peak increased as evidence for the increase in the size distribution of the dispersion. Furthermore, a transient new population, a small “bump” of 110–120 nm in size, appeared after 4 h of exposure and started to decrease in concentration after 8 h. The MALLS signal, which

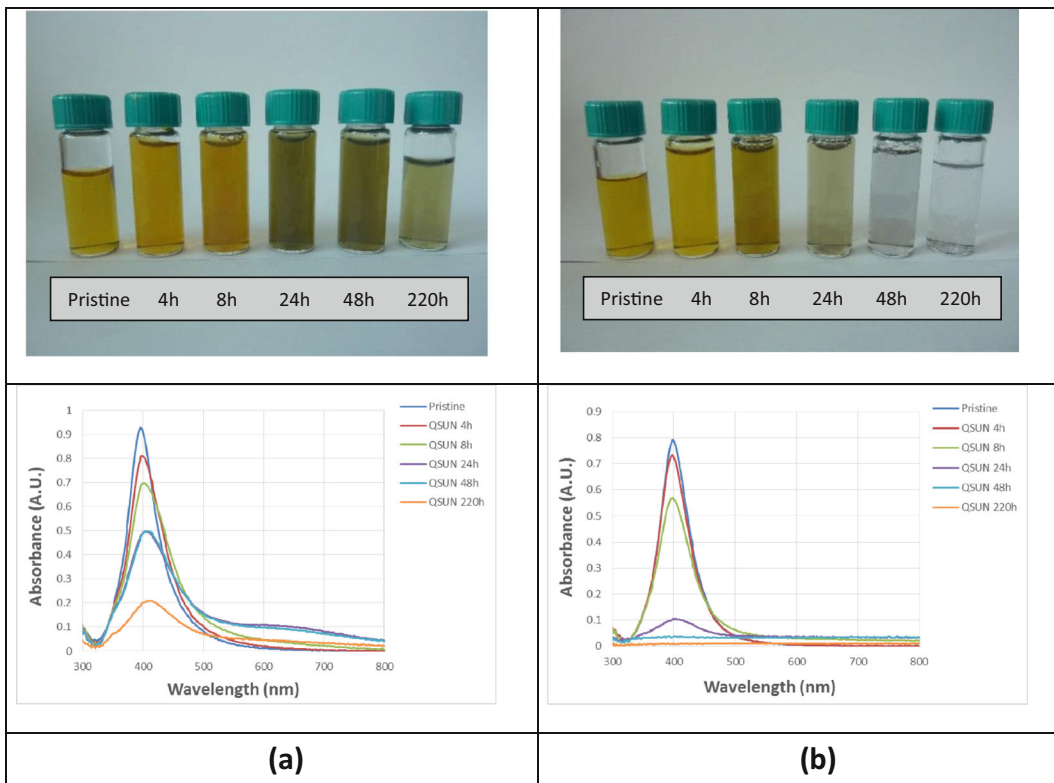


Fig. 1 Alteration of the suspensions of Ag NPs according to exposure time (top) and evolution of the absorbance spectra of Ag NP suspensions (bottom) for **a** Ag Cit and **b** Ag PEG. Dilution factor: 6 for Ag Cit and 10 for Ag PEG in UP water

favors larger particles, clearly showed the occurrence of this second newly formed population. Based on the areas of the ICP-MS peaks obtained, the larger sized population at 8 h of aging had a maximum mass contribution of 14%. Conversely, the Ag PEG fractograms showed a shift in the size distribution towards smaller sizes resulting in a decrease of the mean diameter of the main population from 44 nm before aging to 32 nm at 8 h of exposure and a substantial increase in the mass of

particles smaller than 20 nm. No secondary populations were observed but rather a progressive tailing of the peak towards larger diameters, particularly after 8 h of exposure. It is clear that major transformations of the suspension occurred from this time on, which is reflected in the rapid decrease of the major peak height as well as scattering of the data points on the MALLS signal at diameters above 150 nm. This scattering of the data is likely due to flocculation involving large clusters

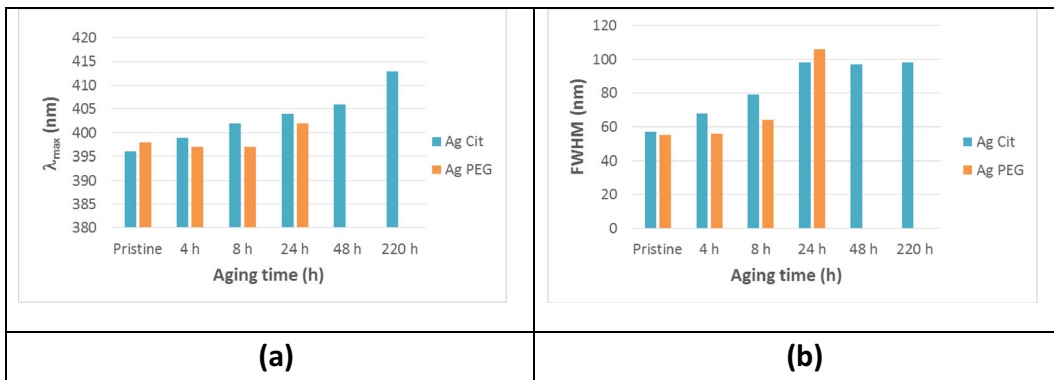


Fig. 2 Evolution of **a** the absorption band maximum (λ_{max}) and **b** the full width at half maximum (FWHM) with time of aging

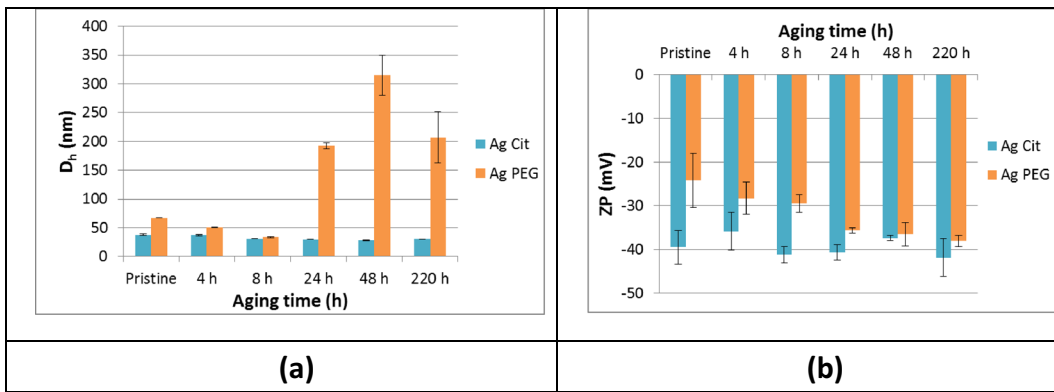


Fig. 3 DLS characterization of the Ag NPs suspensions during the aging process. **a** Hydrodynamic diameter (D_h) and **b** zeta potential (ZP). Experimental conditions: dilution factor: 10 in

1 mM NaNO_3 , $\text{pH} = 6.5 \pm 0.5$. For precipitate-containing suspensions, homogenization was performed by sonication for 1 min to re-disperse the precipitate

that were not completely eluted in the analytical conditions used due to interactions with the separation membrane. These results are in agreement with the DLS data that also detected large particles after 8 h of exposure.

It can be noted that the diameter deduced from the fractograms (D_t) is in agreement with the TEM size obtained for the pristine Ag Cit population but it was

twice the TEM size obtained for the Ag PEG, similarly to the results obtained with DLS. The main reason for such discrepancy lies in the fact that TEM images show the Ag core of the particles only, regardless of the PEG chains grafted on them. As already discussed, the polymer layer thickness can extend from approximately 7 to 24 nm depending on its conformation. A second—and

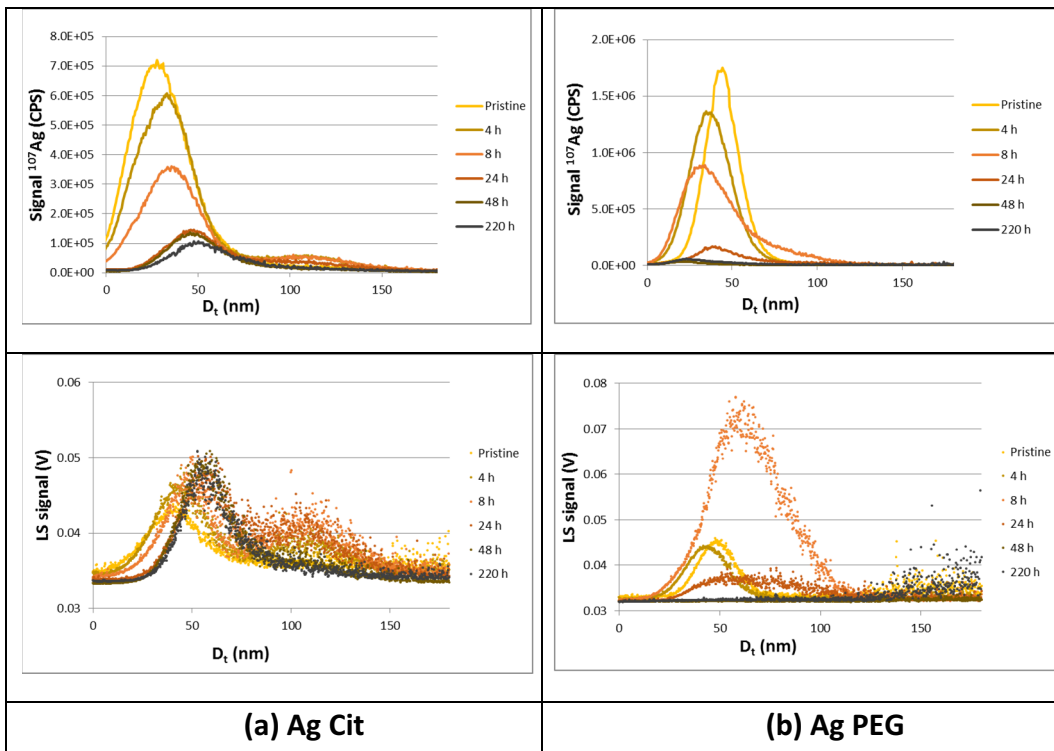


Fig. 4 Fractograms of the Ag NPs suspensions: evolution of their distribution in size with exposure time by on-line ICP-MS (signal of ^{107}Ag , top) and on-line MALLS (signal of 90° detector,

bottom). **a** Ag Cit and **b** Ag PEG. D_t refers to the geometric diameter after elution time calibration of the AF4 with Ag NPs of sizes 20 to 90 nm (TEM estimates)

probably minor—reason cannot be excluded: the nature of the particle surface is identical to that of the set of Ag NPs used for size versus elution time calibration for Ag Cit but different for Ag PEG, which may alter the AF4 elution process for the latter by changing the interactions with the membrane of the separation channel.

Because of the separation mode of the AF4, ionic silver in the injected sample was eluted through the membrane during the focus phase, and the area under the peak of the ICP-MS fractogram is directly proportional to the mass-based concentration of Ag NPs that remain in the sample, regardless of their size. Hence, we can have an indirect estimate of the dissolution rate of the particles by measuring the area of the peak on the fractogram that accounts for the particulate form of silver only. Figure 5 shows the evolution of the peak area (normalized with regard to the initial fractogram of the pristine Ag NPs) with time of exposure. Ag Cit concentration decreased faster than Ag PEG in the first hours of aging (by 40% for the former compared to 12% for the latter at 8 h of aging). The kinetics of dissolution changed between 8 h and 24 h, where the decrease in particulate Ag (in mass) decreased faster for Ag PEG than for Ag Cit. The extremely low peak areas at 48 h and 220 h for Ag PEG reflect the rapid sedimentation of the black deposit in the corresponding vials (Fig. 1b, top).

The initial rates of dissolution for both types of NPs can be assessed by calculating the slope of the curves (here, between $t = 0$ and $t = 8$ h). Time constants of $k_{\text{Ag Cit}} = 0.0496 \text{ h}^{-1}$ and $k_{\text{Ag PEG}} = 0.0154 \text{ h}^{-1}$ were obtained, meaning that Ag Cit dissolves approximately three times faster than Ag PEG at the beginning of the aging process. The acceleration of the rate of particle mass decrease for Ag PEG after the first 8 h of exposure suggests that the PEG capping agent no longer played its protective role regarding Ag NP dissolution.

TEM

In order to better characterize the particles for morphology and chemical composition, TEM observations were proposed. Some relevant images are given in Fig. 6.

The pristine Ag Cit suspension was organized into loose clusters of mostly spherical, 5–50 nm primary particles along with the same scattered single particles (Fig. 6a). After 48 h of sunlight irradiance, the density of particles within the agglomerates looked higher and some edge-cut polygons and triangular nanoplates

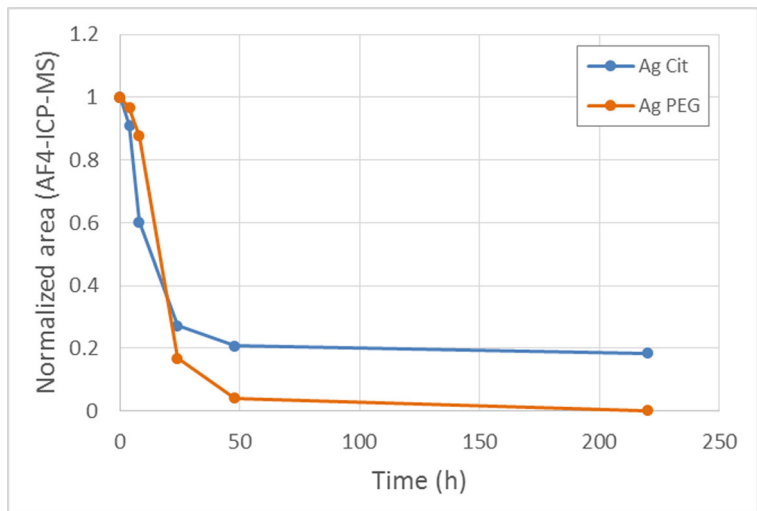
occurred. These particles had an average size of 100 ± 25 nm ($n = 10$), based on spherical equivalent particles, and they likely correspond to the small signal increase observed by AF4 at ca. 110 nm in diameter (Fig. 6b). The diffraction images of these truncated nanoprisms obtained by high-resolution TEM are characteristic of the face-centered cubic system identical to the pristine particles. The polygons looked more eroded after 220 h of aging, and some merged to form larger particles of lower aspect ratio (Fig. 6c), which co-existed with distinct spherical particles. The average diameter of these scattered particles (excluding prisms) was measured at 36 ± 11 nm ($n = 108$), in fair agreement with the AF4-ICP-MS size distribution mode of 47 nm. There was no evidence of extended bridging between these particles. Some of the particles were also found to be embedded in large micrometric structures. EDS analysis of these structures revealed that they were composed of silica (Fig. SI.1) arising from the dissolution of the glassware as already observed in similar experimental conditions (Motellier et al. 2018).

In the case of the pristine Ag PEG, the NPs were homogeneously distributed on the TEM grid, forming a web-like network composed of PEG molecules (Fig. 6d). Remarkably, all the particles seemed to be more or less equally distributed in space with an inter-particle distance of 5–20 nm, close to the PEG conformational extension dimensions (Flory radius of 6.7 nm and “brush” height of 23.7 nm for 5000 MW PEG). Upon the first hours of aging, the web-like layout of the particles disappeared to form compact clusters-containing unchanged particles along with bridged particles of worm-like or branch-like morphologies (Fig. 6e). At 48 h of aging, the primary particles were 26 ± 11 nm ($n = 106$) in diameter, close to that deduced from AF4-ICP-MS analysis (24 nm). Large micrometric polymer-like structures of silica with very small (a few nanometers) Ag NPs attached to them were also observed (Fig. 6e, left). Typical triangular morphologies were found in the aged Ag PEG samples but less so than in the Ag Cit case. The size of these clusters increased with time to finally form micrometric Ag particulate structures (Fig. 6f).

Degradation pathways

The results discussed above have shown that citrate-stabilized Ag NPs and PEG-capped Ag NPs do not follow the same routes and kinetics of aging and yield

Fig. 5 Evolution of the concentration of suspended particles (mass-based from AF4-ICP-MS area of the fractograms)



different degradation products. The early aging process for electrostatically stabilized Ag Cit was likely driven

by oxidative dissolution, as reflected by the early decrease in the peak area of the ICP-MS fractogram

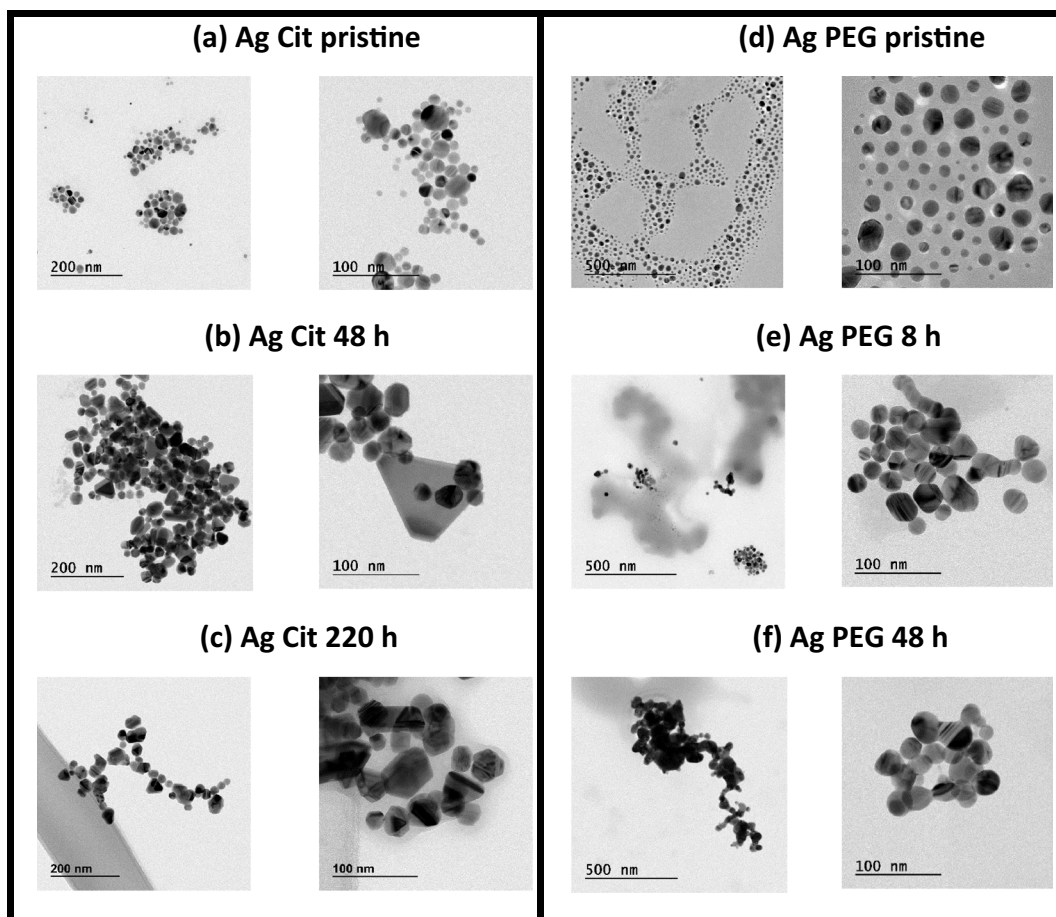


Fig. 6 TEM images of pristine and aged Ag NPs at different sunlight irradiation times. **a, b, c** Ag Cit; **d, e, f** Ag PEG

(Fig. 4a, top and Fig. 5). The initial shift in the population size distribution towards larger sizes was tentatively assigned to the fact that the smallest particles dissolve more rapidly than the largest ones due to a higher surface/volume ratio (Ma et al. 2012), enhanced by the Ostwald ripening process that accounts for the final increase in size of the major spherical population at the end of the aging process (Gentry et al. 2011; Pillai and Kamat 2004; Zhang et al. 2013). During this initial stage, electrostatic repulsion provided by the citrate ions prevented the particles from colliding and aggregating. Then, the reducing properties of citrate promoted the transformation of the free Ag^+ released by the initial dissolution process into $\text{Ag}(0)$ seeds, which were converted into 2D nanoprisms through anisotropic growth under sunlight irradiation, to a relatively low extent (14% maximum after 8 h according to AF4-ICP-MS analysis). The occurrence of these well-faceted particles has been observed in many instances where Ag NP samples were submitted to light irradiance (Callegari et al. 2003; Jin et al. 2001). They were found to be responsible for the color change of the suspension: for instance, green and blue shades correspond to truncated triangular nanoplates similar to those shown in Fig. 6b for Ag Cit at 48 h of aging (Jin et al. 2001; Jin et al. 2003). In the present experiment, this population was transient: at the ultimate exposure time of 220 h, the 2D structures were eroded into particles of undefined shape that co-existed with stabilized initial particles of 50 nm in diameter in the suspension. This whole process can be compared to the evolution of monodisperse 20 nm-, 60 nm-, and 100 nm Ag NPs stabilized with citrate in similar aging conditions (Motellier et al. 2018). Because of the wider size distribution of the present Ag Cit, the evolution of this population features characteristics of the evolutions observed for monodisperse populations: the smallest particles dissolved rapidly and formed Ag seeds that transformed into nanoprisms, which were further eroded and finally precipitated. Some of the initial particles (around 50 nm in diameter) were stabilized with the mediation of SiO_2 structures from the glass, while aggregation prevailed for the largest particles, for which dissolution kinetics was slow.

Contrary to citrate, which is weakly (electrostatically) bound to the core of the Ag particles, PEG is strongly (covalently) grafted to the particle surface (Tejamaya et al. 2012). Despite its potential permeability, the protective PEG layer prevented Ag PEG from experiencing rapid Ag^+ ion release at the

beginning of exposure, in agreement with the enhanced stability of sterically-stabilized NPs compared to electrostatically stabilized NPs (Li et al. 2012). Dissolution occurred to some extent, as evidenced by the 12% decrease of the area of the ICP-MS fractogram peak after 8 h of aging (Fig. 4b, top and Fig. 5). The substantial shift of the Ag PEG population towards smaller sizes may be assigned in part to this first stage of the dissolution process of the silver core, probably initiated at surface spots where the PEG coverage was deficient, but we believe that the primary alteration of the Ag PEG particles was a photo-oxidative deterioration of the polymer shell. Under thermal and UV exposure in air, PEG chains are known to form radicals that cause main chain scission and crosslinking (Rabek 2012). These cleavage reactions induce severe changes in the morphology of the polymer chains (Das and Gupta 2005) and yield degradation products, mainly small carboxylic acids such as glycolic, acetic, oxalic, and formic acids (Giroto et al. 2010; Madera et al. 2003). The convergence of ZP values of Ag PEG towards the stable values of Ag Cit during aging is further evidence for the damage of the PEG capping agent and the increase of the negative surface charge of the particles. In a second step, particles bridged to one another and formed worm- or branch-like structures. The formation of chain-like aggregates has already been observed in chloride-containing medium and was supposedly assigned to secondary AgCl deposits (Li et al. 2010; Li et al. 2012). The same morphologies were also found with light irradiation of bare (Li et al. 2013) and PVP-coated Ag NPs (Cheng et al. 2011). Dipole-dipole interaction arising from the oscillating electrons of the conduction band under electromagnetic solicitation is potentially responsible for inter-particle aggregation. However, this phenomenon cannot be solely responsible for the aggregation pattern of Ag PEG in our experimental conditions as it occurred independently from the type of coating. PEG has been used extensively as a solvent and catalyst in redox reactions (Chen et al. 2005). In the present experiments, the thiol group of PEG-SH was effective in anchoring the stabilizing chain moieties of the polymer to the Ag core, thus preventing their desorption and allowing their interpenetration and/or compression when two particles approached one another (Napper 1977). Given the reducing properties of the small acids generated by the photochemical degradation of the polymer chains and their availability close to the particle surface, PEG is supposed to play a mediating role in the

reduction of dissolved Ag⁺ ions diffusing from the Ag NP core through the PEG layer. We therefore hypothesize that excrescences of Ag(0) were being produced step by step within the PEG shell. This progressive reduction is expected to proceed along the polymer bristles of the “brush”-like structures, between interpenetrating neighboring particles where the PEG chain density and the concentration of the degradation products were the highest, until they finally merged via bridges to obtain the coalescence pattern observed. This plausible mechanism, which is diffusion-limited, is likely to occur at a gradually accelerating rate as the PEG chain density was reduced or even as holes in the protective PEG coating occurred, favoring subsequent Ag⁺ ion release from the bare Ag surface of the core in direct contact with the medium.

Eventually, as the aging proceeded, the PEG became less efficient in preventing the Ag NPs from dissolving. Simultaneously, SiO₂ colloids emerged in solution from the glassware dissolution and some seemed to contribute to some extent to the Ag⁺ ions reduction and stabilization (Mohr et al. 2001; Motellier et al. 2018; Timpel et al. 1997).

Conclusions

The nature of the stabilizing agent was shown to yield separate pathways of Ag NP colloid alteration when exposed to sunlight. The electrostatic-stabilizing citrate-promoted particle morphology changes but postponed the final sedimentation step. Conversely, the initial protecting role of the steric-stabilizing PEG was found to be annihilated by the photodegradation of the polymer chains and to eventually favor inter-particle bridging resulting in aggregation and sedimentation. The networked aggregate structures observed with PEG-coated particles have also been observed by mixing Ag NPs with a soil supernatant (Coutris et al. 2012), which suggests that they can also develop with environmentally ubiquitous natural organic matter, such as the redox-active humic substances (Fimmen et al. 2007). Natural organic matter has been shown to induce the transformation of citrate-stabilized Ag NPs into chain-like structures in the dark after adsorption on the particle surface (Zou et al. 2015). In a recent study, bridging interaction mechanism were assigned to positively and negatively charged functional groups of natural organic ligands (Afshinnia et al. 2018). These

substances could possibly play the same mediating role as that played by PEG in our study and could affect the transfer of Ag NPs between the different environmental compartments.

Acknowledgments The authors thank the Joint Research Center (Ispra, Italy) for providing the set of monodisperse silver nanoparticles used for AF4 calibration.

Funding information This study has received funding from the European Union 7th Framework program under grant agreement No. NMP4-LA-2013-310451 (NanoMILE project). The TEM and AF4-MALS-ICP-MS equipment are part of the NanoID platform supported by the French Investissement d’Avenir ANR-10-EQPX-39.

Compliance with ethical standards

Conflict of interest The authors declare that they have no conflict of interest.

References

- Afshinnia K, Marrone B, Baalousha M (2018) Potential impact of natural organic ligands on the colloidal stability of silver nanoparticles. *Sci Total Environ* 625:1518–1526. <https://doi.org/10.1016/j.scitotenv.2017.12.299>
- Azodi M, Sultan Y, Ghoshal S (2016) Dissolution behavior of silver nanoparticles and formation of secondary silver nanoparticles in municipal wastewater by single-particle ICP-MS. *Environ Sci Technol* 50:13318–13327. <https://doi.org/10.1021/acs.est.6b03957>
- Baalousha M, Stolpe B, Lead JR (2011) Flow field-flow fractionation for the analysis and characterization of natural colloids and manufactured nanoparticles in environmental systems: a critical review. *J Chromatogr A* 1218:4078–4103. <https://doi.org/10.1016/j.chroma.2011.04.063>
- Callegari A, Tonti D, Chergui M (2003) Photochemically grown silver nanoparticles with wavelength-controlled size and shape. *Nano Lett* 3:1565–1568. <https://doi.org/10.1021/nl034757a>
- Chen J, Spear SK, Huddleston JG, Rogers RD (2005) Polyethylene glycol and solutions of polyethylene glycol as green reaction media. *Green Chem* 7:64–82. <https://doi.org/10.1039/B413546F>
- Cheng Y, Yin L, Lin S, Wiesner M, Bernhardt E, Liu J (2011) Toxicity reduction of polymer-stabilized silver nanoparticles by sunlight. *J Phys Chem C* 115:4425–4432. <https://doi.org/10.1021/jp109789j>
- Chiolerio A, Sangermano M (2012) In situ synthesis of Ag-acrylic nanocomposites: tomography-based percolation model, irreversible photoinduced electromigration and reversible electromigration. *Mater Sci Eng B* 177:373–380. <https://doi.org/10.1016/j.mseb.2011.12.029>
- Coutris C, Joner EJ, Oughton DH (2012) Aging and soil organic matter content affect the fate of silver nanoparticles in soil.

- Sci Total Environ 420:327–333. <https://doi.org/10.1016/j.scitotenv.2012.01.027>
- Cumberland SA, Lead JR (2009) Particle size distributions of silver nanoparticles at environmentally relevant conditions. *J Chromatogr A* 1216:9099–9105. <https://doi.org/10.1016/j.chroma.2009.07.021>
- Das I, Gupta SK (2005) Polyethylene glycol degradation by UV irradiation. *Indian J Chem* 44:1355–1358
- Dubascoux S, Le Hecho I, Hasselov M, Von der Kammer F, Gautier MP, Lespes G (2010) Field-flow fractionation and inductively coupled plasma mass spectrometer coupling: history, development and applications. *J Anal At Spectrom* 25: 613–623. <https://doi.org/10.1039/b927500b>
- Fabrega J, Luoma SN, Tyler CR, Galloway TS, Lead JR (2011) Silver nanoparticles: behaviour and effects in the aquatic environment. *Environ Int* 37:517–531. <https://doi.org/10.1016/j.envint.2010.10.012>
- Fernández-López C, Mateo-Mateo C, Álvarez-Puebla RA, Pérez-Juste J, Pastoriza-Santos I, Liz-Marzán LM (2009) Highly controlled silica coating of PEG-capped metal nanoparticles and preparation of SERS-encoded particles. *Langmuir* 25: 13894–13899. <https://doi.org/10.1021/la9016454>
- Fimmen R, Cory R, Chin Y, Trouts T, Mc Knight D (2007) Probing the oxidation-reduction properties of terrestrially and microbially derived dissolved organic matter. 71. <https://doi.org/10.1016/j.gca.2007.04.009>
- Gentry ST, Kendra SF, Bezpalko MW (2011) Ostwald ripening in metallic nanoparticles: stochastic kinetics. *J Phys Chem C* 115:12736–12741. <https://doi.org/10.1021/jp2009786>
- Giddings J (1993) Field-flow fractionation: analysis of macromolecular, colloidal, and particulate materials. *Science* 260: 1456–1465. <https://doi.org/10.1126/science.8502990>
- Giroto JA, Teixeira ACSC, Nascimento CAO, Guardani R (2010) Degradation of poly(ethylene glycol) in aqueous solution by photo-Fenton and H₂O₂/UV processes. *Ind Eng Chem Res* 49:3200–3206. <https://doi.org/10.1021/ie9015792>
- Hagendorfer H, Kaegi R, Parlinska M, Sinnet B, Ludwig C, Ulrich A (2012) Characterization of silver nanoparticle products using asymmetric flow field flow fractionation with a multi-detector approach – a comparison to transmission electron microscopy and batch dynamic light scattering. *Anal Chem* 84:2678–2685. <https://doi.org/10.1021/ac202641d>
- Jiang XC, Chen CY, Chen WM, Yu AB (2010) Role of citric acid in the formation of silver nanoplates through a synergistic reduction approach. *Langmuir* 26:4400–4408. <https://doi.org/10.1021/la903470f>
- Jin R, Cao Y, Mirkin CA, Kelly KL, Schatz GC, Zheng JG (2001) Photoinduced conversion of silver nanospheres to nanoprisms. *Science* 294:1901
- Jin R, Charles Cao Y, Hao E, Metraux GS, Schatz GC, Mirkin CA (2003) Controlling anisotropic nanoparticle growth through plasmon excitation. *Nature* 425:487–490. <https://doi.org/10.1038/nature02020>
- Jokerst JV, Lobovkina T, Zare RN, Gambhir SS (2011) Nanoparticle PEGylation for imaging and therapy. *Nanomedicine (London, England)* 6:715–728. <https://doi.org/10.1038/nature02020>
- Kaegi R, Sinnet B, Zuleeg S, Hagendorfer H, Mueller E, Vonbank R, Boller M, Burkhardt M (2010) Release of silver nanoparticles from outdoor facades. *Environ Pollut* 158:2900–2905. <https://doi.org/10.1016/j.envpol.2010.06.009>
- Krajczewski J, Joubert V, Kudelski A (2014) Light-induced transformation of citrate-stabilized silver nanoparticles: photochemical method of increase of SERS activity of silver colloids. *Colloids Surf A Physicochem Eng Asp* 456:41–48. <https://doi.org/10.1016/j.colsurfa.2014.05.005>
- Krajczewski J, Kołataj K, Kudelski A (2015) Light-induced growth of various silver seed nanoparticles: a simple method of synthesis of different silver colloidal SERS substrates. *Chem Phys Lett* 625:84–90. <https://doi.org/10.1016/j.cplett.2015.02.037>
- Lee H, de Vries AH, Marrink S-J, Pastor RW (2009) A coarse-grained model for polyethylene oxide and polyethylene glycol: conformation and hydrodynamics. *J Phys Chem B* 113: 13186–13194. <https://doi.org/10.1021/jp9058966>
- Levin CS, Bishnoi SW, Grady NK, Halas NJ (2006) Determining the conformation of thiolated poly(ethylene glycol) on Au nanoshells by surface-enhanced Raman scattering spectroscopic assay. *Anal Chem* 78:3277–3281. <https://doi.org/10.1021/ac060041z>
- Li X, Lenhart JJ (2012) Aggregation and dissolution of silver nanoparticles in natural surface water. *Environ Sci Technol* 46:5378–5386. <https://doi.org/10.1021/es204531y>
- Li X, Lenhart JJ, Walker HW (2010) Dissolution-accompanied aggregation kinetics of silver nanoparticles. *Langmuir* 26: 16690–16698. <https://doi.org/10.1021/la101768n>
- Li X, Lenhart JJ, Walker HW (2012) Aggregation kinetics and dissolution of coated silver nanoparticles. *Langmuir* 28: 1095–1104. <https://doi.org/10.1021/la202328n>
- Li Y, Zhang W, Niu J, Chen Y (2013) Surface-coating-dependent dissolution, aggregation, and reactive oxygen species (ROS) generation of silver nanoparticles under different irradiation conditions environmental. *Sci Technol* 47:10293–10301. <https://doi.org/10.1021/es400945v>
- Ma R, Levard C, Marinakos SM, Cheng Y, Liu J, Michel FM, Brown GE Jr, Lowry GV (2012) Size-controlled dissolution of organic-coated silver nanoparticles environmental. *Sci Technol* 46:752–759. <https://doi.org/10.1021/es201686j>
- Madera M, Höflinger W, Kadnar R (2003) Ion chromatographic identification and quantification of glycol degradation products. *J Chromatogr A* 997:279–284. [https://doi.org/10.1016/S0021-9673\(03\)00060-8](https://doi.org/10.1016/S0021-9673(03)00060-8)
- Maillard M, Huang P, Brus L (2003) Silver nanodisk growth by surface plasmon enhanced photoreduction of adsorbed [Ag⁺]. *Nano Lett* 3:1611–1615. <https://doi.org/10.1021/nl034666d>
- Marsh D, Bartucci R, Sportelli L (2003) Lipid membranes with grafted polymers: physicochemical aspects. *Biochim Biophys Acta Biomembr* 1615:33–59. [https://doi.org/10.1016/S0005-2736\(03\)00197-4](https://doi.org/10.1016/S0005-2736(03)00197-4)
- Misra SK, Dybowska A, Berhanu D, Luoma SN, Valsami-Jones E (2012) The complexity of nanoparticle dissolution and its importance in nanotoxicological studies. *Sci Total Environ* 438:225–232. <https://doi.org/10.1016/j.scitotenv.2012.08.066>
- Mitrano DM, Rimmelé E, Wichser A, Emi R, Height M, Nowack B (2014) Presence of nanoparticles in wash water from conventional silver and nano-silver textiles. *ACS Nano* 8: 7208–7219. <https://doi.org/10.1021/nn502228w>
- Mitrano DM, Motellier S, Clavaguera S, Nowack B (2015) Review of nanomaterial aging and transformations through

- the life cycle of nano-enhanced products. *Environ Int* 77: 132–147. <https://doi.org/10.1016/j.envint.2015.01.013>
- Mitrano DM, Lombi E, Dasilva YAR, Nowack B (2016) Unraveling the complexity in the aging of nanoenhanced textiles: a comprehensive sequential study on the effects of sunlight and washing on silver nanoparticles. *Environ Sci Technol* 50:5790–5799. <https://doi.org/10.1021/acs.est.6b01478>
- Mohr C, Dubiel M, Hofmeister H (2001) Formation of silver particles and periodic precipitate layers in silicate glass induced by thermally assisted hydrogen permeation. *J Phys Condens Matter* 13:525–536
- Motellier S, Péliissier N, Mattei J-G (2018) Aging of silver nanocolloids in sunlight: particle size has a major influence. *Environ Chem* 15:450–462. <https://doi.org/10.1071/EN18056>
- Murali VS, Wang R, Mikoryak CA, Pantano P, Draper R (2015) Rapid detection of polyethylene glycol sonolysis upon functionalization of carbon nanomaterials. *Exp Biol Med* 240:1147–1151. <https://doi.org/10.1177/1535370214567615>
- Napper DH (1977) Steric stabilization. *J Colloid Interface Sci* 58: 390–407. [https://doi.org/10.1016/0021-9797\(77\)90150-3](https://doi.org/10.1016/0021-9797(77)90150-3)
- Pillai ZS, Kamat PV (2004) What factors control the size and shape of silver nanoparticles in the citrate ion reduction method? *J Phys Chem B* 108:945–951. <https://doi.org/10.1021/jp037018r>
- Pinzaru I, Coricovac D, Dehelean C, Moacă EA, Mioc M, Baderca F, Sizemore I, Brittle S, Marti D, Calina CD, Tsatsakis AM, Şoica C (2018) Stable PEG-coated silver nanoparticles – a comprehensive toxicological profile. *Food Chem Toxicol* 111:546–556. <https://doi.org/10.1016/j.fct.2017.11.051>
- Rabek JF (2012) Photodegradation of polymers: physical characteristics and applications. Springer Science & Business Media, Berlin
- Rajan K, Roppolo I, Chiappone A, Bocchini S, Perrone D, Chiolerio A (2016) Silver nanoparticle ink technology: state of the art. *Nanotechnol Sci Appl* 9:1–13
- Reidy B, Haase A, Luch A, Dawson K, Lynch I (2013) Mechanisms of silver nanoparticle release, transformation and toxicity: a critical review of current knowledge and recommendations for future studies and applications. *Materials* 6:2295
- Römer I, White TA, Baalousha M, Chipman K, Viant MR, Lead JR (2011) Aggregation and dispersion of silver nanoparticles in exposure media for aquatic toxicity tests. *J Chromatogr A* 1218:4226–4233. <https://doi.org/10.1016/j.chroma.2011.03.034>
- Römer I, Gavin AJ, White TA, Merrifield RC, Chipman JK, Viant MR, Lead JR (2013) The critical importance of defined media conditions in *Daphnia magna* nanotoxicity studies. *Toxicol Lett* 223:103–108. <https://doi.org/10.1016/j.toxlet.2013.08.026>
- Römer I, Wang ZW, Merrifield RC, Palmer RE, Lead J (2016) High resolution STEM-EELS study of silver nanoparticles exposed to light and humic substances. *Environmental Science & Technology* 50:2183–2190. <https://doi.org/10.1021/acs.est.5b04088>
- Tang B, Sun L, Li J, Zhang M, Wang X (2015) Sunlight-driven synthesis of anisotropic silver nanoparticles. *Chem Eng J* 260:99–106. <https://doi.org/10.1016/j.cej.2014.08.044>
- Tejamaya M, Römer I, Merrifield RC, Lead JR (2012) Stability of citrate, PVP, and PEG coated silver nanoparticles in ecotoxicology media. *Environ Sci Technol* 46:7011–7017. <https://doi.org/10.1021/es2038596>
- Timpel D, Scheers Schmidt K, Garofalini SH (1997) Silver clustering in sodium silicate glasses: a molecular dynamics study. *J Non-Cryst Solids* 221:187–198. [https://doi.org/10.1016/S0022-3093\(97\)00333-5](https://doi.org/10.1016/S0022-3093(97)00333-5)
- Vance ME, Kuiken T, Vejerano EP, McGinnis SP, Hochella MF Jr, Rejeski D, Hull MS (2015) Nanotechnology in the real world: redeveloping the nanomaterial consumer products inventory. *Beilstein J Nanotechnol* 6:1769–1780. <https://doi.org/10.3762/bjnano.6.181>
- Yu S, Yin Y, Chao J, Shen M, Liu J (2014) Highly dynamic PVP-coated silver nanoparticles in aquatic environments: chemical and morphology change induced by oxidation of Ag⁰ and reduction of Ag⁺. *Environ Sci Technol* 48:403–411. <https://doi.org/10.1021/es404334a>
- Zhang W, Qiao X, Qiu X, Chen Q, Cai Y, Chen H (2013) Controllable synthesis and Ostwald ripening of silver. *Nanoparticles* 9. <https://doi.org/10.2174/1573413711309060012>
- Zou X, Shi J, Zhang H (2015) Morphological evolution and reconstruction of silver nanoparticles in aquatic environments: the roles of natural organic matter and light irradiation. *J Hazard Mater* 292:61–69. <https://doi.org/10.1016/j.jhazmat.2015.03.005>

Publisher's note Springer Nature remains neutral with regard to jurisdictional claims in published maps and institutional affiliations.